Available online at www.sciencedirect.com
ScienceDirect
Applied Catalysis B: Environmental 83 (2008) 221–228
APPLIED CATALYSIS B: ENVIRONMENTAL
www.elsevier.com/locate/apcatb

Gel-combustion synthesis of nanocrystalline spinel catalysts for VOCs elimination

U. Zavyalova [a,*], B. Nigrovski [a], K. Pollok [b], F. Langenhorst [b], B. Müller [c], P. Scholz [a], B. Ondruschka [a]

[a] *Institute of Technical Chemistry and Environmental Chemistry, Friedrich-Schiller-University Jena, Lessingstrasse 12, D-07743 Jena, Germany*
[b] *Institute of Geosciences, Friedrich-Schiller-University Jena, Germany*
[c] *Institute of Physical Chemistry, Friedrich-Schiller-University Jena, Germany*

Received 21 December 2007; received in revised form 11 February 2008; accepted 13 February 2008
Available online 23 February 2008

Abstract

Gel-combustion synthesis (GCS) in self-sustaining mode was used for preparation of mixed oxide with spinel structure AB_2O_4 (where A = Co, Cu and B = Cr, Co). To support these mixed oxides on CeO_2 and ZrO_2 powders, the GCS technique in self-propagating mode was developed. The synthesized materials were characterized by IR-spectroscopy, X-ray diffraction and transmission electron microscopy. The GCS preparation leads to the formation of nanocrystalline, single-phase spinel catalysts, which showed high activity in VOCs (hexane) elimination. The best catalytic performance was obtained over copper cobaltite catalyst prepared by GCS from glycerin-chelated precursor.

Keywords: Gel-combustion synthesis; Spinel catalyst; Nanocrystalline films; VOCs removal

1. Introduction

Driven by the need for decreasing manufacturing cost and increasing resistance to poisoning of commercial catalysts for volatile organic compounds (VOCs) elimination, efforts have been made to develop metal oxide catalysts, which can exhibit activity similar or higher than of noble metal catalysts [1]. Among them, Co, Cu, Cr, and Mn oxides are the most frequently used for total oxidation of hydrocarbons [2,3]. Improved properties of mixed oxides against individual oxides are well known, especially in the environmental catalysis. In particular, $CuCo_2O_4$ and $CoCr_2O_4$ spinels were found to be very active for CO and hydrocarbons oxidation [4–6], as well as for catalytic removal of NO_x and diesel soot [7]. Furthermore, synergetic effects in Co-based mixed oxide catalysts have been reported, which were rationalised on the basis of enhanced electron transfer and oxygen non-stoichiometry in these oxides [8].

Obviously, the preparation methods play a crucial role in the catalytic performance of the mixed oxides [9,10]. The primary goal of the preparation is an optimizing of the synthesis conditions to obtain oxide catalysts with desired crystal structure as well as high specific surface area. On the other hand, the catalytic reaction often occurs on defects, structure of which is however not well understood and/or identified. Therefore, another objective in the synthesis of oxide catalysts is to produce defect-rich nanocrystalline materials in a controllable manner.

In this paper, we report on the gel-combustion synthesis (GCS) of powdered and supported Co-based mixed oxide catalysts. This approach combines the advantages of sol–gel technique, such as obtaining pure-phase mixed oxides with a good control of stoichiometry and nanoparticle size, and combustion method enabling production of highly defective materials. The difference from the conventional sol–gel process is that in this case chelating agents used in organic complexes serve also as a fuel to maintain the combustion process between oxidant (metal nitrates) and reducing agents (citric acid, glycine, ethylenediamine, etc.). In such a way, the precursor decomposition and the oxide formation are realized by means of high-exothermic combustion reactions and thus differs completely from the usual calcinations.

Previously, we have shown that the effect of Co precursors and fuels, such as urea, citric acid, glycine, and glycerin, on

* Corresponding author.
E-mail address: ulyana.zavyalova@gmail.com (U. Zavyalova).

0926-3373/$ – see front matter © 2008 Elsevier B.V. All rights reserved.
doi:10.1016/j.apcatb.2008.02.015

activity of the combustion-synthesized catalysts in hydrocarbons oxidation correlates well with the combustion behaviour of reactant mixtures [11]. Spinel Co-oxide catalysts with the best catalytic properties were obtained from glycine/nitrate and glycerin/nitrate equimolar mixtures at the lowest synthesis temperatures and the highest synthesis velocities. In contrast to the urea–nitrate combustion method [12], an improvement of metal oxide dispersion can be explained also in terms of the chelating ability of the organic ligands with metal species which prevents unwanted aggregation processes [13]. Since glycine and glycerin are smaller molecules than citric acid or EDTA, a lower temperature requirement for precursor decomposition with an oxide formation is expected. Moreover, taking into account environmental aspect, glycerin is favorable fuel for the combustion synthesis due to the decrease of toxic NO_x emissions during the preparation. Hence, glycerin and glycine were chosen as the fuels for the preparation of nanocrystalline Co-based mixed oxides in this work.

In this paper, the ceria and zirconia supported as well as unsupported spinel catalysts prepared by GCS were studied in total oxidation of *n*-hexane as a VOC molecule. In particular, the factors influencing the structure and reactivity of the spinel catalysts are discussed.

2. Experimental

2.1. Catalyst preparation

Fig. 1 shows the general flow chart for the synthesis of both unsupported and supported catalysts, including catalytic films and coatings. Impregnation is used for powdered supports while monoliths, foams, etc., can be covered by precursors via dip-coating.

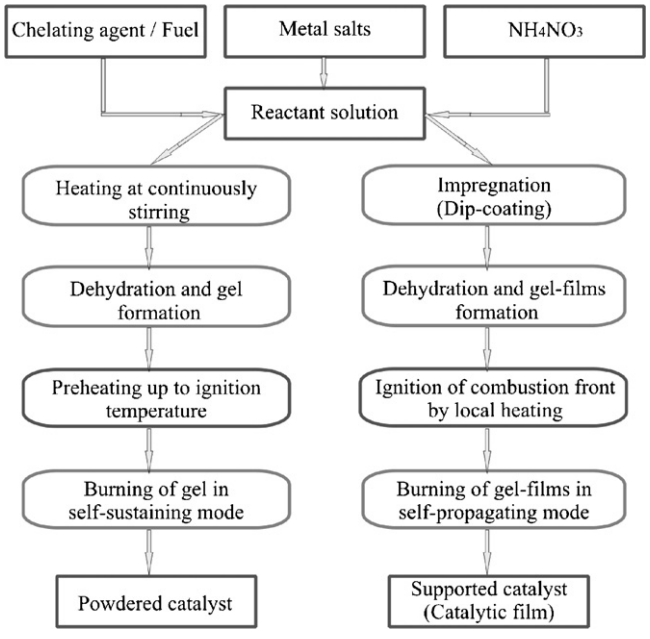

Fig. 1. Flow chart for the preparation of bulk and supported metal oxides by GCS method.

The initial reactant mixtures contained aqueous solutions of Co, Cr, and Cu nitrates with molar ratio Cu:Co = 1:2 and Co:Cr = 1:2 and stoichiometric amounts of glycine or glycerin as fuels. Ammonium nitrate, serving also as additional combustion aid, was only used in few preparations (see below). The homogeneously mixed solution was placed in a quartz pot, heated to 60 °C and continuously stirred using a magnetic agitator for several hours to remove the excess of water. Then, the solution heated to about 80 °C and stirred constantly, transforms into a deep-violet gel. Slow heating of the gel up to 180 °C results in an auto-combustion process with a formation of black fluffy material. The reaction is noticeably exothermic, which leads to a thermal peak in the reacting solid mixture above 1000 °C for a few seconds. The sample was then calcined at 400 °C to ensure the absence of carbonaceous residues which may remain in the samples.

Commercial ceria powder (high purity 15% yttrium-doped CeO_2, S_{BET} = 160 $m^2\ g^{-1}$, from Aldrich) and zirconium oxide powder (high purity 8% yttrium-doped ZrO_2, S_{BET} = 140 $m^2\ g^{-1}$, from Aldrich) were used as supports.

The GCS method was modified for the preparation of the metal oxide catalytic films as described in details elsewhere [11,14]. As opposed to the volumetric combustion method for powder synthesis, in this case exothermic reactions are carried out in a thin layer covered on a support material, which seems to favor a better dispersion of the metal oxide species. Briefly, the main stages for the synthesis of supported catalysts or thin catalytic films by this technique include: incipient wetness impregnation of support by reactant solution containing metal precursor and organic fuel; drying and formation of gel-films; ignition of combustion reactions by means of electrically heated Ni–Cr wire; burning of gel-films in self-propagating mode with the formation of metal oxide nanoparticles.

Some samples of the as-burnt catalysts were further calcined at 700 °C for 4 h for comparison with the catalysts $CoCr_2O_4$ and $CuCo_2O_4$ (samples CuCo(Nitr) and CoCr(Nitr)) prepared by thermal decomposition of metal nitrates in air at 750 °C for 4 h [15].

The list of the Co-based spinels studied in the present work is given in Table 1.

2.2. Characterization

Infrared (IR) spectra were recorded with a PerkinElmer Spectrum 100 FT-IR spectrometer using the Universal ATR Accessory in the range from 4000 to 650 cm^{-1} with 4 cm^{-1} resolution.

The BET specific surface area (SSA), pore volume, and pore size were determined from the adsorption and desorption isotherms of nitrogen using a Quantachrome Autosorb-1 apparatus (outgas conditions: 350 °C, time 2.7 h).

X-ray powder diffraction analysis (XRD) was performed on a URD-6 (“Freiberger Präzisionsmechanik”, Germany) powder diffractometer with Mo Kα radiation (λ = 70.93165 pm) using a second LiF-monochromator in a 2θ range 5–80° in 0,02° increments. Real structure characterization was performed by Rietveld refinements with qualitative and quantitative phase

Table 1
The Co-based spinel catalysts prepared by GCS method and metal nitrate thermal decomposition

Code name	Catalyst composition	Precursor mixtures	Synthesis
CoCr(Gcn)	$CoCr_2O_4$	$Co(NO_3)_2/Cr(NO_3)_3/C_2H_5NO_2$	GCS in self-sustaining mode
CuCo(Gcn)	$CuCo_2O_4$	$Cu(NO_3)_2/Cr(NO_3)_3/C_2H_5NO_2$	
Co(Gcr)	Co_3O_4	$Co(NO_3)_2/C_3H_5(OH)_3$	
CoCr(Gcr)	$CoCr_2O_4$	$Co(NO_3)_2/Cr(NO_3)_3/C_3H_5(OH)_3$	
CuCo(Gcr)	$CuCo_2O_4$	$Cu(NO_3)_2/Co(NO_3)_2/C_3H_5(OH)_3$	
CoCr(Nitr)	$CoCr_2O_4$	$Co(NO_3)_2/Cr(NO_3)_3$	Nitrate thermal decomposition
CuCo(Nitr)	$CuCo_2O_4$	$Cu(NO_3)_2/Co(NO_3)_2$	(calcination at 750 °C for 4 h)
CoCr(Gcr)/Ce	10 wt.% $CoCr_2O_4/CeO_2$	$Co(NO_3)_2/Cr(NO_3)_3/C_3H_5(OH)_3$	GCS in self-propagating mode
CuCo(Gcr)/Ce	10 wt.% $CuCo_2O_4/CeO_2$	$Cu(NO_3)_2/Co(NO_3)_2/C_3H_5(OH)_3$	
CoCr(Gcr)/Zr	10 wt.% $CoCr_2O_4/ZrO_2$	$Co(NO_3)_2/Cr(NO_3)_3/C_3H_5(OH)_3$	
CuCo(Gcr)/Zr	10 wt.% $CuCo_2O_4/ZrO_2$	$Cu(NO_3)_2/Co(NO_3)_2/C_3H_5(OH)_3$	

analysis of all reflexes. Contributions of a mean crystallite diameter (D) and lattice distortion factors—stress and strain ($\Delta d/d$) to X-ray diffraction line broadening were determined by means of PowderCell software [16,17].

The particle size, morphology and chemical composition of the spinel phases and the supporting oxides were studied by a LEO-922 transmission electron microscopy (TEM) operating at 200 keV. The TEM instrument is equipped with an in-column Omega energy filter and an energy-dispersive X-ray (EDX) detector. The TEM samples were prepared by placing drops of a suspension of sample and acetone onto a Lacey gold grid and allow acetone to evaporize. All TEM images were recorded zero-loss filtered with a slow-scan CCD camera, which eliminates almost all contributions from inelastic scattering and thereby significantly improves the contrast of the high-resolution (HREM) images.

2.3. Activity measurements

Catalytic experiments were carried out at constant temperature and atmospheric pressure in a continuous flow system using a fixed-bed reactor. The activities were evaluated over 200 mg of catalyst diluted in 7 ml of glass beads previously checked to be inactive. Before measuring the conversion as a function of temperature, the catalysts were first activated in flowing air at 450 °C for 4 h. *N*-hexane was chosen as a VOC substance. The total gas flow was set to 100 mL min^{-1}, which gives a global gas hourly space velocity (GHSV) of 30,000 h^{-1}, was composed of 500 vppm of *n*-hexane in a 20/80 vol.% oxygen/nitrogen mixture. After reaching a stable reactant flow, adjusted by Brooks mass-flow controllers and a saturator, the feed gas mixture was passed through the catalyst bed and the temperature was increased from room temperature to 450 °C. Inlet and outlet VOC levels were measured on-line by using an Agilent GC System 6850 equipped with FID and TCD detectors. Organic compounds were analyzed with a CP-SIL 8 capillary column, and CO_2—with a HP-Plot Q column. For examining the catalyst stability under the reaction conditions, the catalytic tests were carried out at constant temperature for 12 h.

3. Results and discussion

3.1. Characterization of the bulk spinel catalysts

Detailed XRD structural analysis using Rietveld refinements revealed that single-phase $CoCr_2O_4$ (ICSD 27507) and $CuCo_2O_4$ (ICSD 63387) spinels were obtained by GCS method from the equimolar metal nitrates/glycerin mixtures and from the metal nitrates/glycine/NH_4NO_3 mixtures with molar ratio 1/1/3, respectively. The samples prepared from glycine/nitrate equimolar mixtures without NH_4NO_3 addition contained not only mixed oxides $CoCr_2O_4$ or $CuCo_2O_4$ (about 75–90%) but also small amounts of individual oxides Co_3O_4 (ICSD 36256), Cr_2O_3 (ICSD 201103), and CuO (ICSD 16025). The structural characteristics, surface area, and the temperature of 50%-conversion of hexane over the prepared catalysts are summarized in Table 2.

According to these results, the GCS method leads to the formation of pure oxide catalysts with high SSA in the absence of any support. Comparing the structural characteristics of the spinels prepared with various fuels shows that the substituted spinels $Co^{II}_{0.7}Cr^{II}_{0.3}Cr^{III}_{1.6}Co^{III}_{0.4}O_4$ and $Cu_{0.95}Co_{2,05}O_4$ were formed from the nitrate/glycerin mixture as compared to the normal $CoCr_2O_4$ and $CuCo_2O_4$ phases obtained by nitrate/glycine combustion. For the glycerin prepared CoCr(Gcr) CoCr(Gcr) samples the mean crystallite size of the spinel phase is about five times lower, and SSA values are by 50–120% higher than those in the glycine prepared CoCr(Gcn) and CoCr(Gcn) samples. Apparently, the less exothermic combustion of the equimolar nitrate/glycerin mixture as compared to nitrate/glycine (as shown by DTA [11]), results in the formation of more highly dispersed mixed oxides. In addition, the twice as higher lattice strain in ''glycerine'' samples may indicate their more defective structure as a result of reduction of particle size.

Careful XRD analysis of the conventionally prepared catalyst using metal nitrate decomposition in air at 600 °C for 4 h revealed only mixtures of single Co, Cu, and Cr oxides. Increasing the calcination temperature to 750 °C, as suggested in [15], leads the CoCr(Nitr) sample to contain besides main $Co^{II}Co^{III}_{0,4}Cr_{1,6}O_4$ spinel phase also about 20% of the Cr_2O_3 single phase. Moreover, the CuCo(Nitr) sample consisted of a

Table 2
Characterization of the spinel Co-based catalysts

Code name	XRD phases	Lattice parameter (Å)	Space group	D, nm (XRD)	$\Delta d/d$[a]	S_{BET} ($m^2\ g^{-1}$)	$T_{50\%}$ (°C)
CoCr(Gcn)	$CoCr_2O_4$	$a = b = c = 8.335$	$F41/d{-}32/m$ (2 2 7)	51	0,004.	66	223
CuCo(Gcn)	$CuCo_2O_4$	$a = b = c = 8.134$	$F41/d{-}32/m$ (2 2 7)	45	0.004	68	217
Co(Gcr)	Co_3O_4	$a = b = c = 8.072$	$F41/d{-}32/m$ (2 2 7)	39	0.004	74	219
CoCr(Gcr)	$Co^{II}_{0.7}Cr^{II}_{0.3}Cr^{III}_{1.6}Co^{III}_{0.4}O_4$	$a = b = c = 8.292$	$F41/d{-}32/m$ (2 2 7)	9	0.008	145	190
CuCo(Gcr)	$Cu_{0.95}Co_{2,05}O_4$	$a = b = c = 8.131$	$F41/d{-}32/m$ (2 2 7)	11	0.008	103	198
CoCr(Nitr)	$Co^{II}Co^{III}_{0,4}Cr_{1,6}O_4$–$Cr_2O_3$	$Co^{II}Co^{III}_{0,4}Cr_{1,6}O_4$: $a = b = c = 8.291$	$F41/d{-}32/m$ (2 2 7)	834	0.004	14	275
		Cr_2O_3: $a = 4.944$; $b = 4.944$; $c = 13.547$	$R32/c{-}$(1 6 7)	933	0.004		
CuCo(Nitr)	Co_3O_4-CuO	Co_3O_4: $a = b = c = 8.073$	$F41/d{-}32/m$ (2 2 7)	125	0.002	17	270
		CuO: $a = 4.683$; $b = 3.414$; $c = 5.123$	C 1 2/c 1 (1 5)	622	0.002		
CoCr(Gcr)/Ce	$CoCr_2O_4$-CeO_2	$CoCr_2O_4$: $a = b = c = 8.164$	$F41/d{-}32/m$ (2 2 7)	4	0.007	173	220
		CeO_2: $a = b = c = 5.400$	$F4/m{-}32/m$ (2 2 5)	24	0.003		
CuCo(Gcr)/Ce	$CuCo_2O_4$-CeO_2	$CuCo_2O_4$: $a = 8.133$	$F41/d{-}32/m$ (2 2 7)	<3	0.037	180	213
		CeO_2: $a = b = c = 5.402$	$F4/m{-}32/m$ (2 2 5)	29	0.004		
CoCr(Gcr)/Zr	ZrO_2	ZrO_2: $a = b = 3.594$; $c = 5.181$	$P42/nmcZ$ (1 3 7)	26	0.004	152	254
CuCo(Gcr)/Zr						164	245

[a] Lattice distortion factor (XRD) determined by means of PowderCell software [16,17].

mixture of 66% of Co_3O_4 and 34% of CuO. The mean crystallite size of the conventional catalysts varied in the range of 125–933 nm, and the SSA was about 14–17 $m^2\ g^{-1}$.

Apparently, the formation of single phase of mixed oxide by GCS method can be explained by the solid–solid interactions in Co:Cr and Cu:Co mixtures already at the stage of complexation processes. In this case, pure phase composites can be obtained after mild thermal treatment at relatively low temperatures because the precursors are mixed homogeneously on a molecular level, so that no bulk diffusion restriction has to be overcome during the phase transformations.

Fig. 2 shows the typical cumulative pore volume and the pore size distribution curves for cobalt chromite prepared with GCS technique and conventional metal nitrate decomposition.

According to the N_2 adsorption–desorption isotherms, the CoCr(Gcn) catalyst possesses a monomodal pore size distribution with 5.7 nm mean pore diameter, 0.10 $cm^3\ g^{-1}$ total pore volume and 66 $m^2\ g^{-1}$ SSA (multipoint BET). The CoCr(Gcr) sample prepared from glycerin-chelated precursor also possesses monomodal pore size distribution with 3.8 nm mean pore diameter, 0.14 $cm^3\ g^{-1}$ total pore volume and SSA of 145 $m^2\ g^{-1}$.

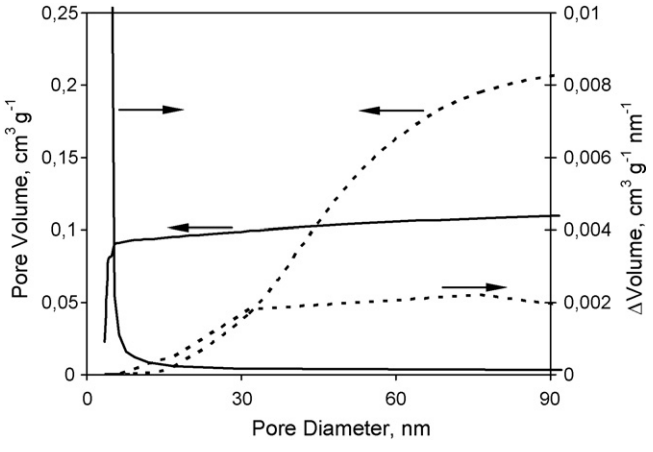

Fig. 2. Pore volume and pore size distribution for the CoCr(Gcr) catalyst (solid line) and CoCr(Nitr) sample (dash line).

As expected, subsequent calcination of the GCS catalysts at 700 °C for 4 h resulted in a decrease of the SSA by about 45%: down to 35–37 $m^2\ g^{-1}$ for CoCr(Gcn) and CuCo(Gcn) catalysts and to 56–78 $m^2\ g^{-1}$ for the CoCr(Gcr) and CuCo(Gcr) samples as a result of particles sintering. However, these annealed GCS catalysts still exhibit a higher dispersion than the CoCr(Nitr) and CuCo(Nitr) samples, which showed a broad pore size distribution with pores centered from 30 to 90 nm (76.4 nm mean pore diameter, 0.20 $cm^3\ g^{-1}$ total pore volume) and SSA of 14 $m^2\ g^{-1}$. It appears that fast combustion process, which accompany by rapid evolution of large quantities of vapours, prevents growth of spinel crystallites, and nano-sized particles with high SSA are formed.

The TEM pictures shown in Fig. 3 indicate a various degree of dispersion for the GCS catalysts prepared from different reactant mixtures. The particle size of the spinel grains in the mixed oxides prepared by glycine/nitrate combustion ranges from 40 to 60 nm (Fig. 3c), which is in agreement with the mean crystallite size determined by XRD. Spinel catalysts obtained from glycerin/nitrate are characterized by particles of about 5–9 nm in size (Fig. 3d and e). The Co-based spinels are magnetic, which renders the high-resolution images very difficult. Therefore, the HREM images are blurred, and it is hard to determine the crystal phases precisely. According to the chemical analysis by EDX, the stoichiometric $CoCr_2O_4$ spinel phase was obtained.

The catalyst prepared by metal nitrate thermal decomposition is characterized by idiomorphic single crystals with

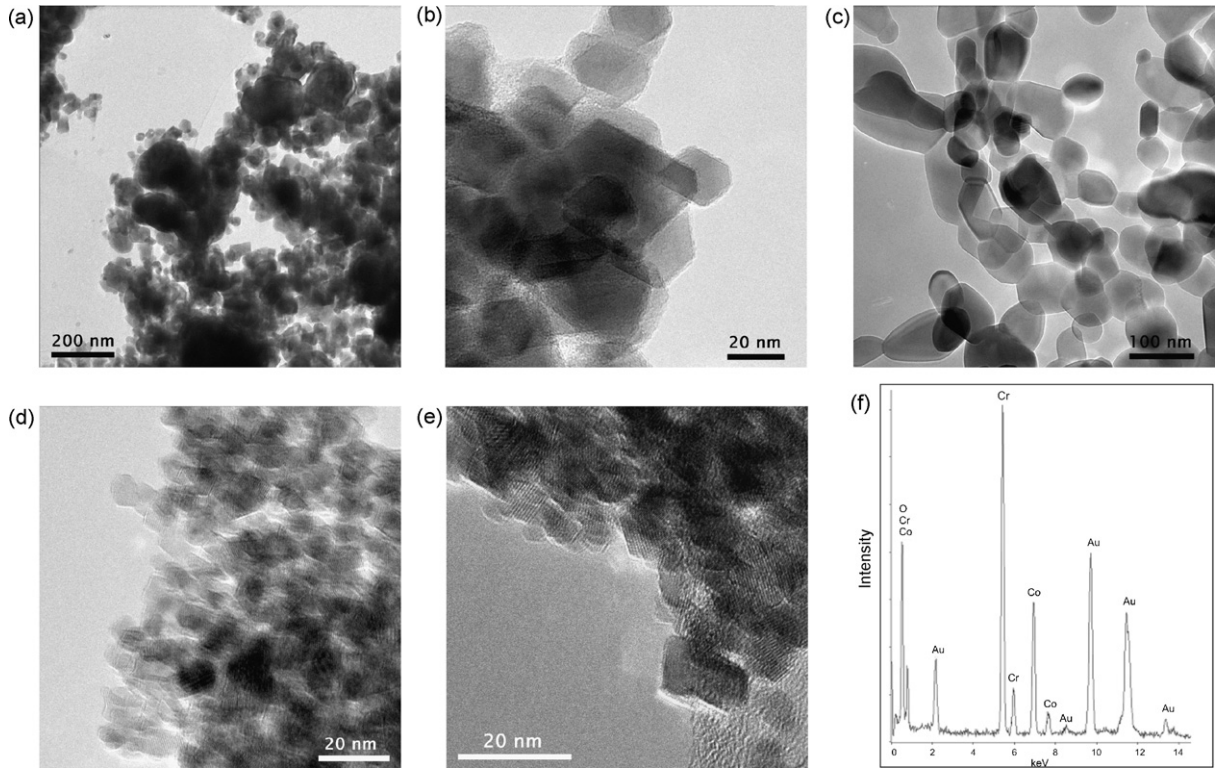

Fig. 3. TEM pictures of cobalt chromite catalysts prepared by various methods: (a and b) CoCr(Nitr); (c) CoCr(Gcn); (d and e) CoCr(Gcr); (f) EDX-spectrum of the CoCr(Gcr).

variable diameter from 20 to a few hundreds nanometers (Fig. 3a and b). Some adjacent crystals share the same orientation which may explain the considerably higher particle size determined by XRD.

3.2. Supported GCS catalysts

In order to disperse the spinel catalysts on CeO_2 and ZrO_2 supports, which are less reactive with Co than Al_2O_3 or SiO_2, the commercial supports stabilized by an yttrium oxide (see Section 2.1) were used. For supported catalyst, the GCS method was used in self-propagating mode [11,14] (see Fig. 1).

The precursor decomposition was controlled by FTIR-analysis of the supported spinel catalysts after various treatments. The results for CeO_2-supported cobalt chromite are shown in Fig. 4.

According to the spectrum (c) in Fig. 4, the ceria support contains water and organic species even after calcination at 400 °C for 4 h. After coating of the support by equimolar glycerin/nitrate mixture, drying, and combustion synthesis in self-propagating mode, the sample still contains small traces of water (OH stretching at 3370 cm^{-1}) and organic compounds (1567/1322 cm^{-1}: NO_2 functional groups) (spectrum b, Fig. 4). Calcination of the as-burnt catalyst at 400 °C for 4 h results in the complete precursor decomposition (spectrum a, Fig. 4).

It is important, that the SSA of the supported spinel catalysts prepared by GCS method increases in all cases by 8–17% as compared to the pure supports and amounts to 152–164 and 173–180 $m^2\ g^{-1}$ for the ZrO_2 and CeO_2-supported catalysts, respectively. This means that the spinel phase does not affect the pore structure of the support.

Fig. 5 shows XRD patterns of 10 wt.% $CuCo_2O_4/CeO_2$ catalysts prepared by GCS method from various reactant mixtures. The particle size of the supported spinel in the sample prepared by glycine/nitrate combustion is about 5 nm, whereas for the sample obtained from glycerin/nitrate the diffraction peaks of the supported component could not be resolved by XRD. For zirconium oxide-supported CoCr(Gcr)/Zr and

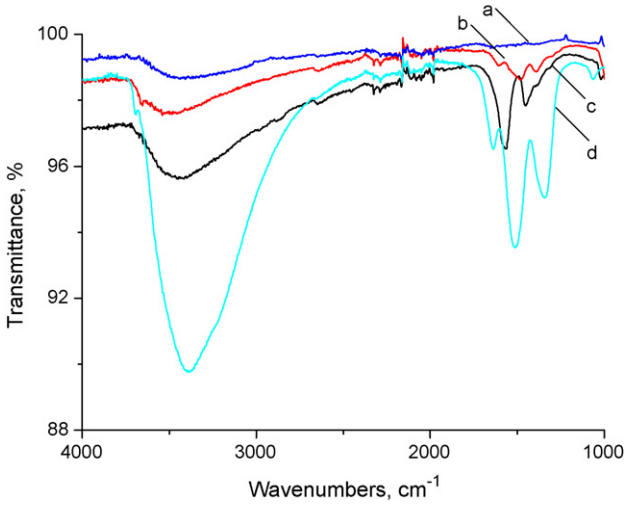

Fig. 4. IR-spectra of CoCr(Gcr)/Ce catalyst after various treatments: (a) catalyst calcined at 400 °C for 4 h; (b) as-burnt sample; (c) initial CeO_2(Y) support calcined at 400 °C for 4 h.

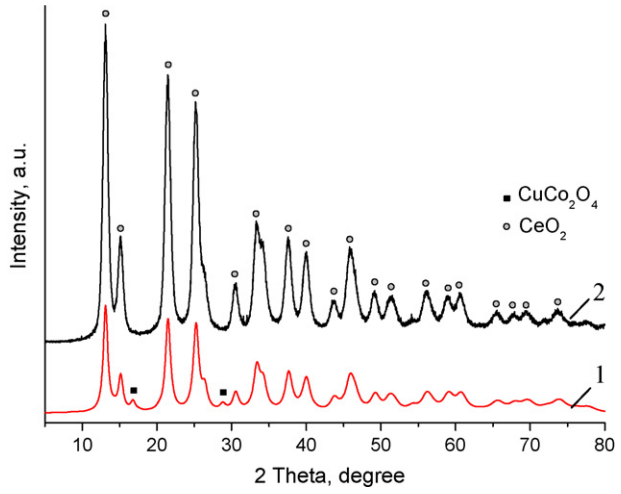

Fig. 5. XRD patterns of 10 wt.% $CuCo_2O_4/CeO_2$ catalysts prepared by GCS method: 1, from glycine/nitrate; 2, from glycerin/nitrate.

CuCo(Gcr)/Zr catalysts only the ZrO_2 peaks were detected by XRD (see Table 2).

XRD analysis shows the reduction of crystallite size for the supported copper cobaltite from 11 nm to below 3 nm, and for the supported cobalt chromite from 9 to 4 nm. The lattice parameter for cobalt chromite catalysts changed from $a = 8.292$ Å to $a = 8.164$ Å for the bulk and supported samples, respectively. This may be due to the particle size effect. However, the lattice parameters of the support materials are also slightly changed. Therefore, the interaction of spinel particles with the support cannot be excluded.

Fig. 6 shows the TEM image of the ceria supported copper cobaltite, prepared from glycine/nitrate. The EDX analysis revealed that almost all particles in this image showed the Co:Cu ratio about 2, which is consistent with a $CuCo_2O_4$ stoichiometry of the supported component. Again, the TEM images were blurred due to the magnetic behaviour of the sample, however, one can estimate the particles size of about 5 nm. Moreover, the crystallites (if any) in the samples prepared from glycerin/nitrate were too small to be detected by XRD and TEM.

It appears that high exothermic combustion wave on the support in self-propagating mode induces rapid formation of oxide nanoparticles, the aggregation of which is inhibited due to the rapid decrease in temperature after the wave propagation. Under these conditions, the uniformly dispersed nano-sized or may be amorphous oxide particles with defect-rich structure can be obtained, as evidenced by observation of very high lattice strain, for example in the CuCo(Gcr)/Ce catalyst about 0.037 (see Table 2).

3.3. Catalytic performance

3.3.1. Unsupported Co-based spinels

Fig. 7 shows the temperature dependences of hexane conversion into CO_2 over copper cobaltite and cobalt chromite catalysts prepared by GCS from glycine/nitrate and glycerin/nitrate mixtures. In all catalytic tests no partial oxidation products were observed and the selectivity in CO_2 was 100%.

The oxidation reaction with the GCS catalysts emerges at about 180–200 °C, and nearly complete combustion of the molecule was achieved at 230–245 °C. Comparison of the temperature profiles in this figure reveals that activity of the Co-based spinel catalysts in the hexane oxidation reaction follows as $CuCo_2O_4 > Co_3O_4 > CoCr_2O_4$. It was previously suggested, that the synergetic effect observed in Co–Cu mixed oxide catalysts might be due to enhanced electron transfer [18–20]. Following this approach, the higher catalytic activity of copper cobaltite catalysts with inverse spinel structure could be also explained in our case by facile electron transfer between divalent Co and Cu cations both occupying the octahedral coordination sites.

There is a clear difference between the catalytic performances of the mixed oxides prepared by GCS from various fuels. Fig. 7 shows that the samples synthesized from glycerin/nitrate mixtures are more active as compared to the catalysts prepared from glycine/nitrate. It is noteworthy that the

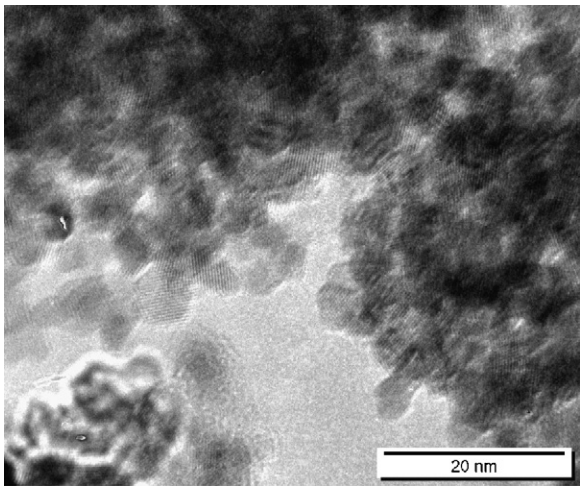

Fig. 6. TEM picture of the copper cobaltite spinel supported on CeO_2 prepared by GCS method from glycine/nitrate.

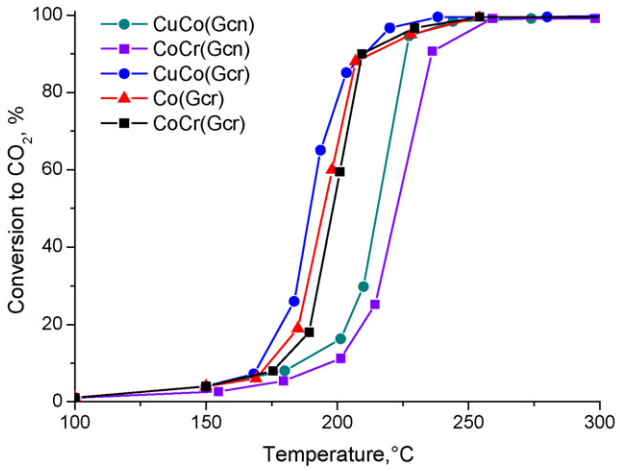

Fig. 7. Conversion of *n*-hexane as a function of reaction temperature over the spinel GCS catalysts prepared from various precursors. Reaction conditions: GHSV = 30,000 h^{-1}; feed: *n*-hexane = 500 vppm balanced by 80% N_2/20% O_2.

interaction of glycerin with metal nitrate in solution is a complex process accompanied with the formation of glycerin associates over a wide range of temperatures and viscosities. However, the observed effect of precursor on the catalytic performance correlates well with their combustion behaviour. Indeed, the glycerin/nitrate solution is characterized by the highest velocity of combustion synthesis and the lowest synthesis temperature [11]. It appears that the GCS conditions – high temperature increase followed by rapid cooling following the combustion process – may assist formation of defect-rich nanocrystalline structures, which contributed to the enhanced activity of this catalyst.

3.3.2. Support effect

To study the support effect on the GCS catalysts pure commercial CeO_2(Y) and ZrO_2(Y) supports and the corresponding 10 wt.% $CuCo_2O_4$ and $CoCr_2O_4$-supported catalysts were tested in hexane total oxidation.

Fig. 8 shows that the CeO_2-supported catalysts are more active for this reaction as compared to the spinels supported on ZrO_2. For the ceria supported samples, the reaction starts at about 180 °C and the complete combustion of hexane is achieved at 280 °C, whereas for the zirconia-supported catalysts 50% conversion of hexane is achieved at about 250 °C, and nearly 100% conversion is completed at 315 °C. It is generally accepted that the oxidation of hydrocarbons on metal oxides proceeds via a redox mechanism, in which the rate-determining step is the oxygen removal from the metal oxide [21,22]. In the Y-doped oxide supports used here, the ability to accumulate oxygen at low temperatures is enhanced due to formation of anionic vacancies [23]. Hence, the redox process may be facilitated in the high-dispersed spinel particles when supported on reducible zirconia and, even better, ceria non-stoichiometric oxides well known for the enhanced oxygen transport.

3.3.3. Thermal and catalytic stability

Fig. 9 shows catalytic performances of cobalt chromite, unsupported and also supported on ceria, for comparison. Then these samples were used in catalytic test at 300 °C for 12 h and

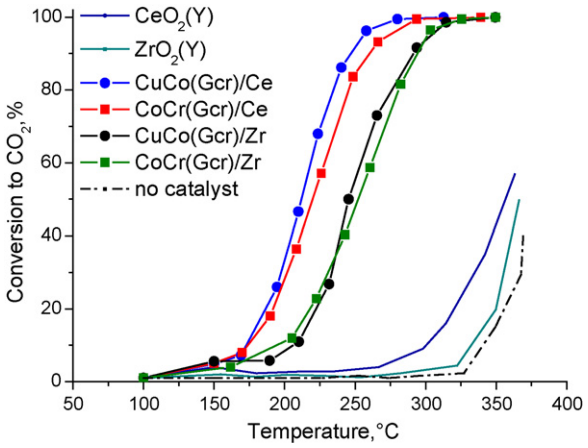

Fig. 8. Hexane conversion over the supported spinel catalyst as indicated. The results for pure support are also shown. *Reaction conditions*: GHSV = 30,000 h^{-1}; feed: *n*-hexane = 500 vppm, balanced by 80% N_2/20% O_2.

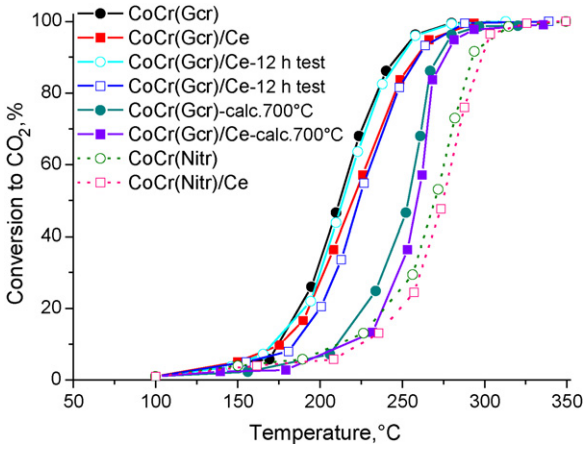

Fig. 9. Temperature dependence of hexane conversion over powder and CeO_2-supported cobalt chromite catalysts after 12 h on stream, and treated at 700 °C for 4 h. Reaction conditions: GHSV = 30,000 h^{-1}; feed: *n*-hexane = 500 vppm, balanced by 80% N_2/20% O_2.

the temperature profile was measured again. The results show no significant changes as compared to the fresh catalysts.

Calcination of the as prepared catalysts at 700 °C for 4 h, which causes sintering as discussed above, leads to significant shift of the $T_{50\%}$ towards higher temperatures. In the latter case, the catalysts behave similar to those prepared by nitrate decomposition, although about 20 °C difference is found between these catalysts for $T_{100\%}$.

It seems plausible that the high catalytic activity of the catalysts prepared by the GCS method cannot be explained exclusively on the basis of increasing surface area. Important factor affecting the activity could be also the formation of mixed oxide of a single phase in contrast to the nitrate thermal decomposition method.

4. Conclusions

In this work, the gel-combustion synthesis, in which chelating agent serves simultaneously as a fuel to maintain the combustion process, has been developed for the preparation of bulk and supported spinel catalysts. This preparation allows one to synthesize highly dispersed mixed oxide catalysts of predominantly single phase. The GCS conditions – high temperature increase followed by rapid cooling in the combustion process – may assist the formation of defect-rich nanocrystalline structures.

We found that catalytic performance of the GCS catalysts in the VOCs (*n*-hexane) elimination correlates with structural and textural properties of the Co-based spinels, which in turns are influenced by the preparation and precursor used. The best catalytic performance in hexane elimination was obtained over copper cobaltite catalyst prepared by combustion of glycerin-chelated metal nitrates.

Acknowledgements

We gratefully acknowledge Dr. J. Schmidt for the textural characterization of the catalysts. U.Z. thanks Prof. P.G. Tsyrulnikov for fruitful discussions.

References

[1] C. Lahousse, A. Bernier, B. Delmon, P. Papaefthimiou, T. Ionnides, X. Verykios, J. Catal. 178 (1998) 178.
[2] S.C. Kim, J. Hazard. Mater. B 91 (2002) 285.
[3] J. Kirchnerova, D. Klvana, Catal. Lett. 67 (2000) 175.
[4] P. Stefanov, I. Avramova, D. Stoichev, N. Radic, B. Grbic, Ts. Marinova, Appl. Surf. Sci. 245 (2005) 65.
[5] D. Fino, N. Russo, G. Saracco, V. Specchia, Catal. Today 117 (2006) 559.
[6] U. Zavyalova, V.F. Tretyakov, T.N. Burdeynaya, V.V. Lunin, A.I. Titkov, A.N. Salanov, P.G. Tsyrulnikov, Petrol. Chem. 45 (4) (2005) 255.
[7] D. Fino, N. Russo, G. Saracco, V. Specchia, J. Catal. 242 (2006) 38.
[8] H.G. El-Shobaky, Appl. Catal. A 278 (2004) 1.
[9] M. Qian, H.C. Zeng, J. Mater. Chem. 7 (1997) 493.
[10] L. Markov, A. Lyubchova, J. Mater. Sci. Lett. 10 (1991) 512.
[11] U. Zavyalova, P. Scholz, B. Ondruschka, Appl. Catal. A 323 (2007) 226.
[12] J. Papavasiliou, G. Avgouropoulos, T. Ioannides, Appl. Catal. B 66 (2006) 168.
[13] F. Wyrwalski, J.-F. Lamonier, S. Siffert, A. Aboukais, Appl. Catal. B 70 (2007) 393.
[14] P.G. Tsyrulnikov, U. Zavyalova, N.B. Shitova, N.D. Ryshova, V.F. Tretyakov, RU Patent 2,284,219 (issued 27/4/2005).
[15] W.M. Shaheen, A.A. Ali, Mater. Res. Bull. 36 (2001) 1703.
[16] W. Kraus, G. Nolze, Program PowderCell for Windows, Berlin, 2000.
[17] B. Müller, W. Kraus, G. Nolze, Zeitschr. Kristall. 19 (2002) 81.
[18] S. Castillo, M. Moran-Pineda, R. Gomez, J. Catal. 172 (1997) 263.
[19] A. Vodyankin, L. Kurina, V. Popov, Kinet. Catal. 40 (1999) 636.
[20] B.L. Yang, S.F. Chang, W.S. Chang, Y.Z. Chen, J. Catal. 130 (1991) 54.
[21] Y.M. Yang, B.Z. Wan, Appl. Catal. A 114 (1994) 35.
[22] B. Ramachandran, H.L. Greene, S. Chatterjee, Appl. Catal. B 8 (1996) 157.
[23] S.P. Kulyova, E.V. Lunina, V.V. Lunin, B.G. Kostyuk, G.P. Muravyova, A.N. Kharlanov, E.A. Jilinskaya, A. Aboukais, Chem. Mater. 13 (2001) 1491.